Title

Asymmetrical Flow Field Flow Fractionation Coupled to Nanoparticle Tracking Analysis for Rapid Online Characterization of Nanomaterials.

Journal

Analytical Chemistry, 92(10)

Authors

Adkins, Gary

Sun, Erica

Coreas, Roxana

et al.

Publication Date

2020-05-19

DOI

10.1021/acs.analchem.0c00406

Peer reviewed

HHS Public Access

Author manuscript

Anal Chem. Author manuscript; available in PMC 2021 May 19.

Published in final edited form as:

Anal Chem. 2020 May 19; 92(10): 7071–7078. doi:10.1021/acs.analchem.0c00406.

Asymmetrical Flow Field Flow Fractionation Coupled to Nanoparticle Tracking Analysis for Rapid Online Characterization of Nanomaterials

Gary Brent Adkins[1], **Erica Sun**[1], **Roxana Coreas**[2], **Wenwan Zhong**[1,2,*]

[1]Department of Chemistry; University of California-Riverside, Riverside, CA 92521.

[2]Environmental Toxicology Graduate Program, University of California-Riverside, Riverside, CA 92521.

Abstract

Increasing applications of nanomaterials in consumer goods, industrial products, medical practices, etc., calls for the development of tools for rapid separation, quantification and sizing of nanoparticles to ensure their safe and sustainable employment. While many techniques are available for characterization of pure, homogeneous nanomaterial preparations, particle sizing and counting remains difficult for heterogeneous mixtures resulted from imperfect synthesis conditions, aggregation responsive to change in distribution solutions, or degradation during storage. Herein, nanoparticle tracking analysis (NTA) was coupled to asymmetrical flow field flow fraction (AF4) using a splitter manifold to enable on-line particle separation and counting. The high pressure and flow rate in AF4 were reduced to the levels compatible with NTA by the proper flow splitting design; and a syringe pump was employed to withdrew fluid through the exit port of NTA and maintain consistent flow rates entering NTA for proper particle sizing. Successful AF4-NTA coupling was demonstrated by analyzing a mixture of polystyrene particles with the average diameters around 50, 100, and 200 nm. Good correlation was observed between the amount of each type of particle injected to and measured by the hyphenated system. The particle concentrations acquired using on-line and off-line coupling of AF4-NTA also agreed well with each other. The non-spherical nanoparticles like gold nanorods and hexagonal boron nitride nanosheets were also analyzed to demonstrate the versatile applicability of this system. Our work has proved that, AF4-NTA can achieve accurate particle counting on different populations of the nanomaterials in a mixture, which cannot be done by either AF4 or NTA alone. It will be a valuable tool for rapid characterization of heterogeneous nanomaterial solutions without purification to fulfill the regulation requirement on the nanomaterial-containing products.

Graphical Abstract

*Corresponding author: Dr. Wenwan Zhong, Wenwan.zhong@ucr.edu.

Supporting Information

The Supporting Information is available free of charge on the ACS Publications website: Data and descriptions showing NTA scripting and AF4 elution methods, batch mode NTA for PS bead mix, single against mixed population injections, and a description of NTA size determination theory of spherical and non-spherical particles.

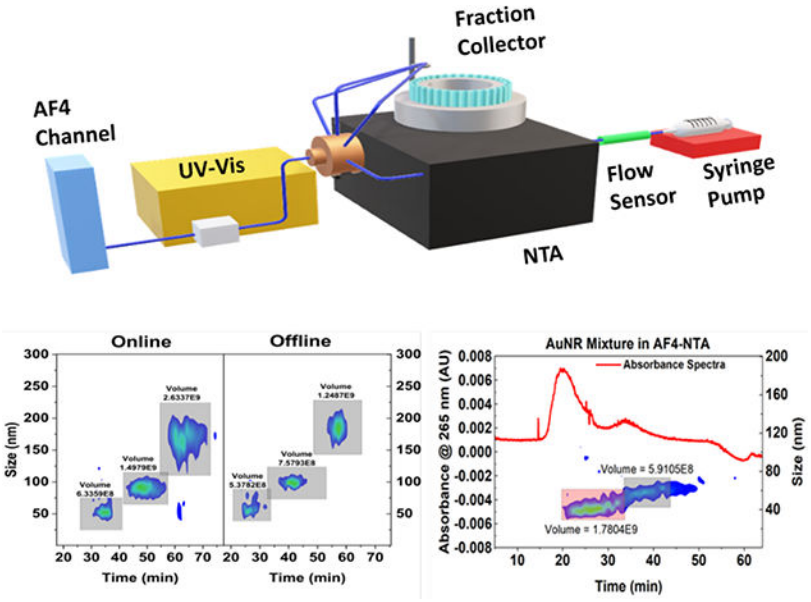

Keywords

Nanoparticle tracking analysis; Asymmetrical flow field flow fractionation; On-line coupling; 2D nanomaterial; Nanoparticles; Characterization

INTRODUCTION

Nanotechnology has been integrated into a wide array of consumer products, urging governing bodies of these markets to adopt guidelines or regulations regarding the reporting and characterization of those nanomaterials due to their possible adverse environmental or biological effects.[1–6] The first nanomaterial reporting and labeling regulation in consumer goods was established by the European Union (EU) for cosmetic products being sold in the EU market in 2009.[7] Specifically, the regulation asks: 1) does a product contain nanomaterials that need to be reported; 2) does the size of the nanomaterial fall within the regulation of 1–100 nm; and 3) what is the number size distribution of the nanomaterials?[8] One of the challenging requirements in this regulation is the determination of a number size distribution. This means the distribution must be generated from counted nanoparticles that have been sized individually and not from measurements of the bulk solution. Similarly, in the US, the Food and Drug Administration (FDA) requires that, if a product contains nanomaterials, specific information about the physiochemical properties, purity, and toxicity of the nanomaterials must be provided.[9] These guidelines also demands that the aggregation and agglomeration properties of the nanomaterials in the product should be revealed.

Several techniques exist to satisfy these regulations, but they are usually technically demanding, involve expensive instruments, and need multiple analyses to perform a full characterization. Offline techniques like transmission electron microscopy (TEM)[10–13], scanning electron microscopy (SEM)[14–20], and atomic force microscopy (AFM)[21–24] can produce number counting as well as size, but these methods are low in throughput and often

require surface adsorption and drying, which may not capture the total concentration or observe the nanoparticles in their native state in the sample matrix. Access may also be limited in many cases due to the cost of instruments capable of the higher resolution needed to detect in the sub 100 nm range. On the other hand, techniques like resistive pulse sensing (RPS), dynamic light scattering (DLS) and multi angle light scattering (MALS) that can individually size nanoparticles suspended in solution are available. But the low sample throughput and variation of the data with respect to the pore size used in RPS complicate data analysis and limit it in rapid nanoparticle quantification.[25,26] DLS and MALS instruments are highly efficient in acquiring particle concentration; and acquire diffusion coefficient (D) via the time dependent scattering intensity fluctuation, which is then used to calculate particle size using the Stokes Einstein equation.[27–28] However, since the intensity of the scattered light rapidly decays with particle diameter, LS-based instruments have difficulties in accurately sizing small particles.

Nanoparticle tracking analysis (NTA) is a recently introduced technique that can count and size nanoparticles down to approximately 30 nm.[25, 29–31] The system uses a fluidic channel on top of a laser module that is angled to achieve total internal reflection. Nanoparticles in the solution will scatter the incident light towards an objective lenses and camera system. The system tracks the mean squared displacement of the particle and determines the diffusion coefficient from the Brownian motion of the particle. By measuring individual particles, NTA generates a histogram that displays accurate nanoparticle concentration and size distributions. This technology avoids data bias from membrane pore size like in RPS. In addition, NTA uses a fluidic channel setup which allows simple fluidic connections, making it a strong candidate to be used as an online detector.

Pairing NTA with a separation system can enhance analysis repeatability and reduce sample complexity. A good choice for this purpose is asymmetrical flow field flow fractionation (AF4) because it combines filtration with size-based separations.[32–34] It uses an open channel design that is constructed with a singular membrane wall.[35] The liquid leaving through the membrane generates a crossflow that presses the analyte close to the membrane. Particles will differentially diffuse against this crossflow towards the center of the channel that relates to the hydrodynamic diameter. Larger analytes diffuse slower and thus stay closer to the membrane wall and move more slowly in the channel; while the smaller ones with higher diffusion coefficients will diffuse against the crossflow more, locating to higher average distances from the membrane surface and eluting faster. AF4 can separate nanomaterials with sizes ranging from nano- to micro-meters by simply adjusting the crossflow to detector flow ratios.

To our knowledge, there has no report for directly coupling AF4 with NTA for particle separation and counting. Herein, we design a simple connection interface between NTA and AF4, and the resultant set-up allows rapid particle separation followed by online concentration and size determination. We have demonstrated that the connection design can successfully reduce the channel back-pressure and direct the eluent from AF4 to NTA at the desired flow rates for accurate particle sizing. This system can handle diverse types of nanomaterials, has good versatility with injection volumes or sample concentrations, and does not require materials to carry labels or modifications for enhanced detectability.

EXPERIMENTAL

Reagents and Materials.

FL-70 detergent (tetrasodium ethylenediamineteraacetate 1.4%, sodium oleate 0.5%, sodium bicarbonate 0.1%, sodium carbonate 2.7%, triethanolamine oleate 3.8%, water 88.8%, polyethylene glycol 0.9%, alcohol, C12–14-secondary, ethoxylated 1.8%), and the polystyrene bead standards were purchased from Thermo Fisher Scientific (Waltham, MA). While the claimed particle sizes were 50 nm, 100 nm, 200 nm (NIST 3000 series), based on the Certificate of Analysis (COA) provided by the manufacturer, the actual size average was measured by NTA to be 50 nm, 96 nm and 180-nm, respectively. However, for convenience they were termed 50-, 100-, and 200-nm beads in this work. NanoXact gold nanorods with the dimensions of 47.6 × 18.0 nm and 103.2 × 18.5 nm were purchased from nanoComposix (San Diego, CA). The 2D nanomaterial of hexagonal boron nitride (hBN) with the average lateral dimension around 150 nm and layer thickness < 10 nm was provided by Engineered Nanomaterials Resource and Coodination center (ERCC), part of NHIR consortium at Harvard HSPH-HIEHS Nanosafety Center. The detailed characterization of which was reported in our previous work.[36] A SLI-0430 Sensirion flow sensor kit was purchased from Newark (Centerville, OH) for NTA flow rate measurements. A 9-port manifold was purchased from Upchurch Scientific (Lakeforest, IL). Ultrapure H_2O (18.2 MΩ) was generated onsite with a Direct-Q 3 UV water purification system (MilliposeSigma; Burlington, MA).

AF4-NTA Coupling Connection.

Procedures for preparation of the nanoparticle solution and the AF4 method used in our analysis can be found in Supporting Information. Scheme 1 shows the fluidic connection of our setup. A 9-port manifold was attached after the UV-Vis detector and before the NTA to split the AF4 line into multiple flow paths, thus reducing the total pressure in each line. One line was attached directly into the Low Volume Flow Cell manifold, while the other three lines were connected to the fraction collector (FC) with equal length tubing. The waste port of the NTA was connected to a New Era NE-500-X syringe pump controlled by Syringe Pump Pro software. The lines were purged of air before equilibration. The desired flow rate was generated by vacuum caused by gently withdrawing the syringe at a preset flow rate (15 μL/min) using the Syringe Pump Pro software.

Nanoparticle Analysis using NTA.

Particle counting was carried out on a Nanosight NS300 from Malvern Panalytical using a low volume flow cell manifold and a 405 nm laser module. The video collection time was determined as 60 s minus the processing time of each video, which was 5 s on the current CPU of the system, making the video collection time 55 s. Detection threshold (DT) was kept at 4, with camera levels being dictated by the particle's optical properties. The video was processed using the Malvern NTA 3.3 software. For mixture analysis, the camera level was reduced in steps over the separation to avoid oversaturation of the camera when larger particles were being measured. For example, when the polystyrene bead mixture was measured, the camera level started at 13 for 20 minutes and then decreased to 10 for 20 minutes, before finally dropping to 6 for the final 20 minutes. A flow sensor was connected

to the exit port of NTA to monitor flow rates throughout the runs. A flow rate of 15 μL/min was induced by a New Era NE-500X syringe pump. Example scripts are shown in the Supporting Information.

Offline analysis was performed using similar conditions, maintaining the video capture time at 55 seconds and DT at 4. Camera levels were dependent on the size and optical properties of the nanoparticle. A Harvard syringe pump was used to push offline samples through the flow cell using arbitrary script settings values. Flow rates were set to 15 μL/min using the generated standard curve (Figure S2) relating script settings to achieved flow rates. A setting of 70 generated a flow of approximately 15 μL/min.

To process the online data files, a summary file containing all 55-s videos for a separation was created by the software that contained each video's distribution. Each video corresponded to the data for that 1-minute interval used in the fractograms. To make the 3D contour plot visually presentable, a baseline of 1×10^6 was set. In each 3D plot, Region of Interest (ROI) boxes were marked, and the particle number counted within each ROI was calculated by multiplying the volumetric particle concentration from each 55-s video (in particles/mL per min) with the elution time of the ROI (in min) and the AF4 detector flow rate before the splitter manifold (0.5 mL/min).

RESULTS AND DISCUSSION

Flow Splitting Design.

The outlet flow rate of AF4 is in the range of 5–0.1 ml/min, which is much higher than the flow in the channel of NTA. Therefore, to use NTA as an online detector, a flow splitter is needed to direct only a small portion of the AF4 eluent to NTA at compatible flow rates. As shown in Scheme 1, we solved this issue by using a multi-port manifold (part C in Scheme 1). The challenge of such a junction design is to maintain a highly consistent flow rate going into the NTA channel, regardless of any flow or pressure changes caused by the AF4 separation. This is because a typical AF4 separation method gradually decreases the crossflow rate to obtain optimal elution times and resolution, in which the system pressure should be varied to maintain a constant outlet flow rate. This dynamic pressure limits the ability to split and control flow with static back pressure regulators, such as smaller ID tubing, or by gravity. In our design, a syringe pump (part E in Scheme 1) is connected to the exit port of NTA to withdraw liquid from NTA at a constant flow rate. Because the flow rate of the tube connected to the NTA system would be much higher than that of the withdrawal rate, the syringe pump acts as a flow regulator. If the system is purged of air, the incompressibility of the fluid acts as a stable back pressure regulator, which helps alleviate any pressure pulses caused by normal switching of the liquid pump check valves.

To maintain a low volume flow rate in the NTA line and accommodate a wide range of system pressure in AF4, a 9-port manifold was employed in our design. A COMSOL simulation was conducted to prove the plausibility of our design (Supporting Information). More ports on the splitter manifold allowed additional FC lines to be opened, which reduced the total pressure in each FC line to be close to atmospheric and eliminated the risk of leakage and damage to the NTA channel. For example, if a system runs at 3–4 bar during

separation, opening 1 NTA line and 3 FC lines is sufficient to keep the total pressure in each line around 1 bar.

In order to decrease band broadening and retention time shifts induced by the drastically different flow rates, the tubing length after the splitter going to the NTA must be reduced to a minimal amount and connected into the “short” end of the channel that feeds directly into the viewing window (See Picture in Supporting Figure S4). Additionally, the lines feeding the FC must be kept at identical lengths or the sample bands would not be delivered at the same time into the collection tubes. Finally, the FC lines must be kept open to atmosphere and not be rejoined using a second manifold to prevent over pressurization of the NTA channel.

The effectiveness of using a syringe pump at the exit port of NTA to control flow rates in NTA while connected to AF4 was tested experimentally against hydrodynamic control, i.e. using the height difference between the NTA and FC exit ports to control the flow rate in the NTA line. Due to continuous pressure change throughout the AF4 separation process, the hydrodynamic control method was not able to maintain steady flow rate and thus would only be accurate for a small range of separation conditions (Figure 1A). In contrast, using a syringe pump provided a nice consistent flow rate over the whole separation. In addition, the minor pulses of the flow rate generated from the check valves were mostly eliminated (Inset of Fig. 1A).

NTA Maximum Flow Rate Determination.

The Malvern NTA 3.3 software measures the speed of Brownian motion (random motion in the x and y direction) of each particle to calculate the size of a particle. Because the particle solution is pulled through the measurement channel by a syringe pump, all particles move towards a constant direction, termed the x-direction drift, while also undergoing Brownian motion, which has the random movement in all directions. The software would measure the x-direction drift caused by the channel flow rate and remove it from each particle’s measurement when computing the particle’s Brownian motion. However, the software can only tolerate a flow rate within a certain range, and exceeding such a range, size and particle number measurements would not be valid. Since the detector flow rate of AF4 is much faster than that tolerable by NTA, and could vary to attain good analyte resolution, we needed to determine the maximum flow rate the hyphenated system can handle. Thus, we connected a flow sensor directly after the NTA exit port to measure the flow rate inside the NTA channel, controlled the syringe pump setting to result in different flow rates (Supporting Figure S4), and investigated the effect of flow rates on analysis of the polystyrene size standards.

The results were displayed in Fig. 1B & C. We found that, the particle concentration (Figure 1B), as well as the size mode (Figure 1C), of the 100- and 200-nm particles decreased as the flow rate increased; while the smaller, 50-nm particles were affected less within this flow rate range. The maximum flow rate was then determined as the rate that could induce 5% change in particle concentration and size mode compared to the average values measured at no flow rate. Using particle concentration, the maximum flow rate for 100- and 200-nm was estimated to be 30.0 μL/min and 27.75 μL/min, respectively, but the change in particle concentration for the 50-nm particles was smaller than 5% in the entire flow rate range

investigated. Using the size mode data, the maximum flow rate for the 50-, 100- and 200-nm particles was found to be, 34.84 μL/min, 31.96 μL/min, and 16.08 μL/min respectively. We can see that, the overall maximum flow rate decreases with increasing particle size. This is probably due to the lower magnitude of Brownian motion with the larger particles that makes the particle x-direction drift corrections less tolerant to higher flow rates. Additionally, larger particles optically flare more, which causes more difficulty in determination of the center of the particle during Brownian motion measurements and results in higher measurement errors from frame to frame. To keep all particle within a 5% error, a flow rate of 15.00 μL/min was employed as the operating flow rate for online NTA analysis in the present work.

Polystyrene Bead Standard Analysis.

The purpose of building the AF4-NTA system is to provide accurate and repeatable counting of each particle population in a nanoparticle mixture. To test the performance of our system, individual injections of the 50-, 100-, and 200-nm polystyrene particles were carried out; and the resultant retention time, peak shape and total particle quantification were compared with those obtained from injection of the mixture of the 3 populations. The contour plots graphing the size, retention time, and particle counts are displayed in Figure S5. No noticeable difference was found between the plots from injections of the mixed and single particle samples. The coefficient of variability (CV %) between particle counts for each particle population was found to be below 5% (Table 1). These results support that our system can perform reproducible particle counting from solutions containing pure or mixed particle populations.

Next, we compared the performance of particle quantification using the stand-alone NTA and the AF4-NTA system. Although the measurement by NTA alone displayed the presence of three particle populations when analyzing the mixture of the particles (Figure S6 in the supporting information), size resolution was poor. Additionally, the peaks for the 50- and 100-nm particles were not reproducible. The 50-nm particle population was not always accurately determined due to the camera level settings: using the optimal camera level for detection of the 50-nm particles resulted in heavy optical flaring of the 200-nm particles, causing many of the 50- and 100-nm particles to be shielded from the camera by the bright flair.

This issue was solved when NTA was coupled to AF4 by decreasing the NTA camera level during the separation process, since the smaller particles were eluted earlier than the larger particles. Three well-separated particle populations were then detected with both the size and concentration information obtained (online analysis, Figure 2A). We also collected the particles eluted after AF4 and measured them by NTA (offline analysis, Fig. 2B). The particle sizes and elution windows measured by the online and offline methods agreed well with each other, with some shifts in retention times due to the different flow rates between the ports of the NTA and FC. The dead-volume of the NTA channel also increased band broadening in the online analysis. Comparing the particle counts shown in Fig. 2A and 2B, the off-line coupling method showed lower measured values. We observed about 15% reduction in the particle counts for the 50-nm particles when measured by the off-line

method compared to the on-line method, and the percent drop increased to 50% for the two larger particles. Because offline analysis requires time for each fraction to be measured (approximately 3 minutes between each fraction), the fractions eluted at later times would sit in the tube for a longer period before being measured by NTA. We suspect the increased time spend in the collection tube may have increased adsorption to the wall of the tube, causing the reduction in particle count in the off-line method. This should be tested in future studies. In addition, the larger particles may have settled out of the solution before being measured by NTA. Based on the Stoke equation, the settling rate of a spherical particle in a fluid (water in our case) is equal to $(\rho_{particle} - \rho_{fluid}) \times d^2 \times g/(18\times \eta)$, with ρ being the density of the particle (1.05 g/cm^3) or water (1.00 g/cm^3), g being the gravity acceleration constant (9.81 m/s^2), d being the particle diameter, and η being the viscosity of water (0.01 g/cm.s). The larger particles would settle at a rate much faster than the smaller ones, which may be accounted for particle loss in the off-line method. But we anticipate this effect was not significant in our case, because only a very small distance (~ 10 μm) could have been travelled during the ~2.5 hrs experiments, even for the largest, 200-nm particles.

Additionally, we evaluated the accuracy of particle quantification using AF4-NTA by injecting different amounts (represented by injection volume of the mix) of the mixed polystyrene particles. The fractograms collected in the UV-Vis detector clearly showed increasing peak areas with increasing injection volumes (Fig. 2C). Agreeing well with the UV-Vis detection, NTA measurement also gave out linear ($R^2 > 0.99$) increase in the detected particle concentration with increasing injection volume (Fig. 2D). Minor deviations between the actual and measured particle concentration could be caused by membrane adsorption during AF4 separation, but with optimal selection of the proper membrane surface and separation condition, particle losses could be minimized.

The results shown in Fig. 2C & D also illustrate the difference in particle detection using NTA and UV-Vis absorption. Using the AF4-NTA system, the limit of detection (LOD) for the 200-nm, 100-nm, and 50-nm particles were 2.84×10^8, 5.19×10^6, and 1.37×10^7, respectively. While in UV-Vis detection, the smaller particles had comparable LODs as in NTA, the 200-nm particles, had an LOD about 8 folds lower than that from NTA. In UV-Vis detection, the larger particles can absorb more light than the smaller ones because of their larger volume per particle leading to a higher molar absorptivity; and the 200-nm ones could even scatter the incident light of 265 nm, leading to a higher absorbance and much better detectability. However, while in the bulk optical methods like UV-Vis detection, the conversion constants such as molar absorptivity would need to be known before the actual particle molar concentration can be determined; NTA allows all particles larger than 30-nm to be measured, with the camera level and DT properly set, which provides an unbiased counting of the particle concentration. Moreover, with NTA providing measurements of sizes, even if the particles of different sizes were not well separated in AF4, size resolution could be improved by connecting it to NTA. Smaller particles that are co-eluted with the larger particle populations can be easily recognized in the 3D contour plot. Though, NTA carries has a narrow dynamic range of particle concentration. NTA calculates particle concentration by taking a simple average of the particles visible per frame and converting it to a particle count per volume of the viewing area (in the scale of nL). The particles should be well apart from each other for clear viewing effect during Brownian motion

measurement, which, plus the small viewing volume, prevents NTA from accurate measurement of particles with concentrations higher than 10^{11} particles/mL.

Non-spherical Nanomaterials.

While the above study was focused on spherical particles, AF4 is highly versatile at analyzing nanomaterials with diverse morphology, owing to its open channel and good accommodation with analytes having wide size ranges. To test this ability, two types of non-spherical particles were analyzed by both the stand-alone NTA and the AF4-NTA system.

Ten μL of the stock AuNRs solutions with the dimensions of 47.6 × 18.0 nm and 103.2 × 18.5 nm (length × diameter) were mixed and diluted to a final particle concentration of 3.2×10^8 and 2.4×10^9 particles/mL, respectively, in 1 mL of the Fl-70 buffer. But, stand-alone NTA was not able to repeatedly reveal the presence of two distinct particle populations in the mixture (Fig. 3A); while AF4-NTA clearly detected two particle populations in the resultant 3D contour plot (Fig. 3B). Even though the peak resolution was not satisfactory, quantification of each particle population can be done based on their elution times and size measurements (Table 2). The ROI box can cover all particles locating within a certain size window as seen in Fig. 3B. We can see from Table 2 that the quantification and sizing results of each NR population measured by the AF4-NTA system agree well with those obtained by the stand-alone NTA on the pure NR solution. These results prove that our system can provide accurate information about the concentration of each particle population in a mixture.

There are some discrepancies between the particle concentration and hydrodynamic size values obtained by NTA and those provided by the manufacturer in the products' COA. The COA particle concentration is calculated based on the mass concentration measured by ICP-MS and the averaged volume and density of the AuNRs; thus, it is understandable that it could vary slightly from that obtained by NTA through counting individual particles. However, the difference in particle size is quite large. The COA values are 13– 15 nm, and determined by DLS, which is much smaller than the 35–37 nm range reported in NTA. This is because DLS uses a different approach to measure particle size than NTA.[27–28] While both instruments calculate particle size using the Stokes Einstein equation from the diffusion coefficient (D), DLS acquires D via the time dependent scattering intensity fluctuation,[27–28] and NTA determines D by tracking the movement of each particle and measuring the average distance it moves in the x and y directions.[29–30] Their different manners in D determination induce relatively larger deviation in measuring the dimension of non-spherical particles like NRs compared to the spherical ones.[37–38] It also has been shown by Žagar and Pahovnik *et al.* that DLS underestimates the size of particles in batch mode as well as flow mode, especially in larger diameter particles.[39]

Analysis of 1 mL of 500 ng/mL hBN solution by standalone NTA exhibited a size distribution covering 50 to 100 nm (Figure 4A). In AF4-NTA (Fig. 4B), the separation showed a wide elution window from 15–45 minutes. Summing the particle numbers detected over the entire separation course yields the true number distribution of the 10 μL hBN stock solution that was injected in the system. Since 1 μL stock solution was used in the diluted stand-alone NTA sample, the particles were normalized to 1 μL of hBN stock solution by

dividing the total particle count by 10. Interestingly, the AF4-NTA was able to measure more of the smaller particles within the size range of 30 to 50 nm compared to stand-alone NTA. Even though the same camera level was used for both AF4-NTA and stand-alone NTA, separating the sample allows the smaller, dimmer particles to be revealed because they are not masked by the larger, brighter particles in solution.

CONCLUSION

A hyphenated system of particle separation by AF4 and sizing by NTA has been developed in the present work for rapid and accurate nanoparticle quantification and characterization. Because AF4 can separate diverse types of analytes falling within a wide size based on their hydrodynamic diameters, this coupling provides a versatile nanoparticle characterization system that also allows collection of separated particle populations for further characterization. Flow rate was shown to be important to the analytical accuracy of the instrument, and a reduction in channel pressure was needed to protect the NTA channel from damage or leaks. The relative simplicity and straightforward nature of the setup and data collection process improves the speed at which this data can be collected and analyzed, generally being able to get quantification data in not much longer than the time a separation would take. NTA has some limitations as an online detector, such as its narrow working range, low flow rates, low pressure thresholds, and a dependence on optimal detector settings, but the added simplicity, efficiency, and unbiased particle counting make NTA an efficient online detector that could be coupled to any fluidic system where pressure and flow rates can be specifically controlled.

Supplementary Material

Refer to Web version on PubMed Central for supplementary material.

ACKNOWLEDGMENT

Research reported in this publication was supported by the National Institute of Environmental Health Sciences of the National Institutes of Health under Award Number U01ES027293 for W. Zhong as part of the Nanotechnology Health Implications Research (NHIR) Consortium. The hBN ENMs presented in this publication were procured/developed, characterized, and provided by the Engineered Nanomaterials Resource and Coordination Core established at Harvard T. H. Chan School of Public Health (NIH grant # U24ES026946) as part of the Nanotechnology Health Implications Research Consortium. R. Coreas was supported by the Research Training Grant in Environmental Toxicology from the National Institute of Environmental Health Sciences (T32ES018827). We are also grateful to the support from the Research Training Grant in Environmental Toxicology from the National Institute of Environmental Health Sciences (T32ES018827) to G. B. A. and R.C.

REFERENCES

(1). Mohammad F; Al-Lohedan HA Toxicity Assessment of Engineered Mn–ZnS Quantum Dots in Vitro. J. Mater. Sci 2016, 51, 9207–9216.

(2). Wang Z; Vijver MG; Peijnenburg WJGM Multiscale Coupling Strategy for Nano Ecotoxicology Prediction. Environ. Sci. Technol 2018, 52, 7598–7600. [PubMed: 29947218]

(3). Bundschuh M; Filser J; Luederwald S; McKee MS; Metreveli G; Schaumann GE; Schulz R; Wagner S Nanoparticles in the environment: where do we come from, where do we go to? Environ. Sci. Eur 2018, 30, 1–17. [PubMed: 29375955]

(4). Simonin M; Richaume A Impact of engineered nanoparticles on the activity, abundance, and diversity of soil microbial communities: a review. Environ. Sci. Pollution Res, 2015, 22, 13710–13723.

(5). Zhang Y; Bai Y; Jia J; Gao N; Li Y; Zhang R; Jiang G; Yan B Perturbation of physiological systems by nanoparticles. Chem.Soc. Rev, 2014, 43, 3762–3809. [PubMed: 24647382]

(6). Ranjan S; Dasgupta N; Singh S; Gandhi M Toxicity and regulations of food nanomaterials. Environ. Chem. Lett, 2019, 17, 929–944.

(7). Bowman DM; van Calster G; Friedrichs S Nanomaterials and Regulation of Cosmetics. Nat. Nanotechnol 2010, 5, 92–92. [PubMed: 20130584]

(8). Contado C Nanomaterials in Consumer Products: A Challenging Analytical Problem. Front. Chem 2015, 3, 48. [PubMed: 26301216]

(9). Office of Cosmetics and Colors. Guidance for Industry: Safety of Nanomaterials in Cosmetic Products | FDA https://www.fda.gov/regulatory-information/search-fda-guidance-documents/guidance-industry-safety-nanomaterials-cosmetic-products#IIIB1.

(10). Ramachandramoorthy R; Bernal R; Espinosa HD Pushing the Envelope of In Situ Transmission Electron Microscopy. ACS Nano 2015, 9, 4675–4685. [PubMed: 25942405]

(11). Michen B; Geers C; Vanhecke D; Endes C; Rothen-Rutishauser B; Balog S; Petri-Fink A Avoiding Drying-Artifacts in Transmission Electron Microscopy: Characterizing the Size and Colloidal State of Nanoparticles. Sci. Rep 2015, 5.

(12). Wang ZL New developments in transmission electron microscopy for nanotechnology. Adv. Mat 2003, 15, 1497–1514.

(13). Bescond A; Yon J; Ouf FX; Ferry D; Delhaye D; Gaffié D; Coppalle A; Rozé C Automated Determination of Aggregate Primary Particle Size Distribution by TEM Image Analysis: Application to Soot. Aerosol Sci. Technol 2014, 48, 831–841.

(14). Barcikowski S; Hahn A; Kabashin AV; Chichkov BN Properties of Nanoparticles Generated during Femtosecond Laser Machining in Air and Water. Appl. Phys. A Mater. Sci. Process 2007, 87, 47–55.

(15). Fissan H; Ristig S; Kaminski H; Asbach C; Epple M Comparison of Different Characterization Methods for Nanoparticle Dispersions before and after Aerosolization. Anal. Methods 2014, 6, 7324–7334.

(16). Mazzoli A; Favoni O Particle Size, Size Distribution and Morphological Evaluation of Airborne Dust Particles of Diverse Woods by Scanning Electron Microscopy and Image Processing Program. Powder Technol. 2012, 225, 65–71.

(17). Bootz A; Vogel V; Schubert D; Kreuter J Comparison of Scanning Electron Microscopy, Dynamic Light Scattering and Analytical Ultracentrifugation for the Sizing of Poly(Butyl Cyanoacrylate) Nanoparticles. Eur. J. Pharm. Biopharm 2004, 57, 369–375. [PubMed: 15018998]

(18). Sitzmann B; Kendall M; Watt J; Williams I Characterisation of Airborne Particles in London by Computer-Controlled Scanning Electron Microscopy. Sci. Total Environ 1999, 241, 63–73.

(19). Saupe A; Gordon KC; Rades T Structural Investigations on Nanoemulsions, Solid Lipid Nanoparticles and Nanostructured Lipid Carriers by Cryo-Field Emission Scanning Electron Microscopy and Raman Spectroscopy. Int. J. Pharm 2006, 314, 56–62. [PubMed: 16574354]

(20). Cox JT; Zhang B Nanoelectrodes: Recent Advances and New Directions. Annu. Rev. Anal. Chem 2012, 5, 253–272.

(21). Gwaze P; Annegarn HJ; Huth J; Helas G Comparison of Particle Sizes Determined with Impactor, AFM and SEM. Atmos. Res 2007, 86, 93–104.

(22). Hoo CM; Starostin N; West P; Mecartney ML A Comparison of Atomic Force Microscopy (AFM) and Dynamic Light Scattering (DLS) Methods to Characterize Nanoparticle Size Distributions. J. Nanoparticle Res 2008, 10 (SUPPL. 1), 89–96.

(23). Kanno T; Yamada T; Iwabuki H; Tanaka H; Kuroda SI; Tanizawa K; Kawai T Size Distribution Measurement of Vesicles by Atomic Force Microscopy. Anal. Biochem 2002, 309, 196–199. [PubMed: 12413451]

(24). Grobelny J; DelRio FW; Pradeep N; Kim DI; Hackley VA; Cook RF Size Measurement of Nanoparticles Using Atomic Force Microscopy. Methods Mol. Biol 2011, 697, 71–82. [PubMed: 21116955]

(25). Maas SLN; de Vrij J; van der Vlist EJ; Geragousian B; van Bloois L; Mastrobattista E; Schiffelers RM; Wauben MHM; Broekman MLD; Nolte-'t Hoen ENM Possibilities and Limitations of Current Technologies for Quantification of Biological Extracellular Vesicles and Synthetic Mimics. J. Control. Release 2015, 200, 87–96. [PubMed: 25555362]

(26). Vaclavek T; Prikryl J; Foret F Resistive Pulse Sensing as Particle Counting and Sizing Method in Microfluidic Systems: Designs and Applications Review. J. Sep. Sci 2019, 42, 445–457. [PubMed: 30444312]

(27). Levin A; Shmytkova E; Khlebtsov B Multipolarization dynamic light scattering of nonspherical nanoparticles in solution. J. Phys. Chem. C 2017, 121, 3070–3077.

(28). Arenas-Guerrero P; Delgado ÁV; Donovan KJ; Scott K; Bellini T; Mantegazza F; Jiménez ML Determination of the Size Distribution of Non-Spherical Nanoparticles by Electric Birefringence-Based Methods. Sci. Rep 2018, 8: 9502. [PubMed: 29934624]

(29). Wright M Nanoparticle Tracking Analysis for the Multiparameter Characterization and Counting of Nanoparticle Suspensions In: Soloviev M (eds) Nanoparticles in Biology and Medicine. Methods in Molecular Biology (Methods and Protocols), 2012, 906, 511–524. Humana Press, Totowa, NJ

(30). Filipe V; Hawe A; Jiskoot W Critical Evaluation of Nanoparticle Tracking Analysis (NTA) by NanoSight for the Measurement of Nanoparticles and Protein Aggregates. Pharm. Res 2010, 27, 796–810. [PubMed: 20204471]

(31). Sokolova V; Ludwig A-K; Hornung S; Rotan O; Horn PA; Epple M; Giebel B Characterisation of Exosomes Derived from Human Cells by Nanoparticle Tracking Analysis and Scanning Electron Microscopy. Colloids Surfaces B Biointerfaces 2011, 87, 146–150. [PubMed: 21640565]

(32). Caputo F; Arnould A; Bacia M; Ling WL; Rustique E; Texier I; Mello AP; Couffin AC Measuring Particle Size Distribution by Asymmetric Flow Field Flow Fractionation: A Powerful Method for the Preclinical Characterization of Lipid-Based Nanoparticles. Mol. Pharm 2019, 16, 756–767. [PubMed: 30604620]

(33). Giddings JC Field Flow Fractionation: A Versatile Method for the Characterization of Macromolecular and Particulate Materials. Anal. Chem 1981, 53, 1170–1178.

(34). Wahlund KG; Giddings JC Properties of an Asymmetrical Flow Field-Flow Fractionation Channel Having One Permeable Wall. Anal. Chem 1987, 59, 1332–1339. [PubMed: 3605623]

(35). Ahn JY; Kim KH; Lee JY; Williams PS; Moon MH Effect of Asymmetrical Flow Field-Flow Fractionation Channel Geometry on Separation Efficiency. J. Chromatogr. A 2010, 1217, 3876–3880. [PubMed: 20439106]

(36). Duan Y; Coreas R; Liu Y; Bitounis D; Zhang Z; Parviz D; Strano M; Demokritou P; Zhong W Prediction of Protein Corona on Nanomaterials by Machine Learning Using Novel Descriptors. NanoImpact 2020, 17, 100207.

(37). Shang J; Gao X Nanoparticle counting: towards accurate determination of the molar concentration. Chem. Soc. Rev 2014, 43, 7267–7278. [PubMed: 25099190]

(38). Maguire CM; Rösslein M; Wick P; PrinaMello A Characterisation of particles in solution – a perspective on light scattering and comparative technologies, Sci. Technol. Advanced Mater 2018, 19, 732–745.

(39). Sitar S; Vezočnik V; Maček P; Kogej K; Pahovnik D; Žagar E Pitfalls in Size Characterization of Soft Particles by Dynamic Light Scattering Online Coupled to Asymmetrical Flow Field-Flow Fractionation. Anal. Chem 2017, 89 (21). 10.1021/acs.analchem.7b03251.

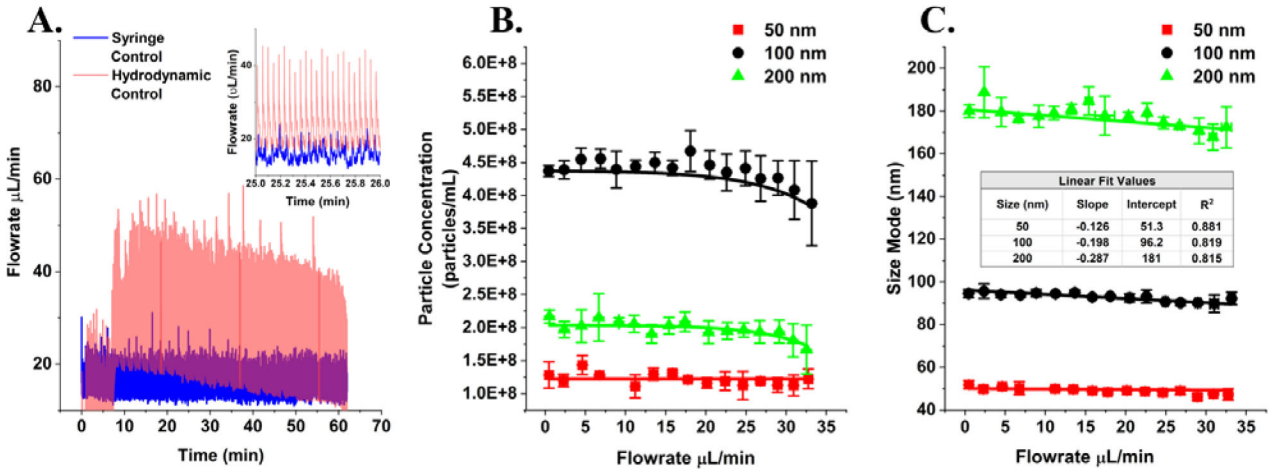

Figure 1.

Flow rate control and maximum flow rate determination. Hydrodynamic-controlled flow rates and syringe pump-controlled flow rates are shown in (A) and a zoomed scale in (Inset). (A) Full run showing variable flow rates due to variable pressures resulting from changing crossflows throughout the run. (Inset) Zoomed in portion showing reduced flow rate fluctuations due to the incompressible fluid in the syringe pump line. (B) Particle concentration maximum flow rate that was determined by the intersection of the linear portions of the exponential function. (C) Maximum flow rates were determined by determining a 5% error tolerance and solving for the value at 0 uL/min flow rate multiplied by 0.95 for size mode. Error bars in Figure 1B and 1C are taken as the standard deviation between the three replicates performed for each bead population. The x-direction error bars are determined as the variance in flowrates achieved using arbitrary settings found in Figure S2. The y-direction error comes from the data generated by NTA in particle size (B) and particle concentration (C).

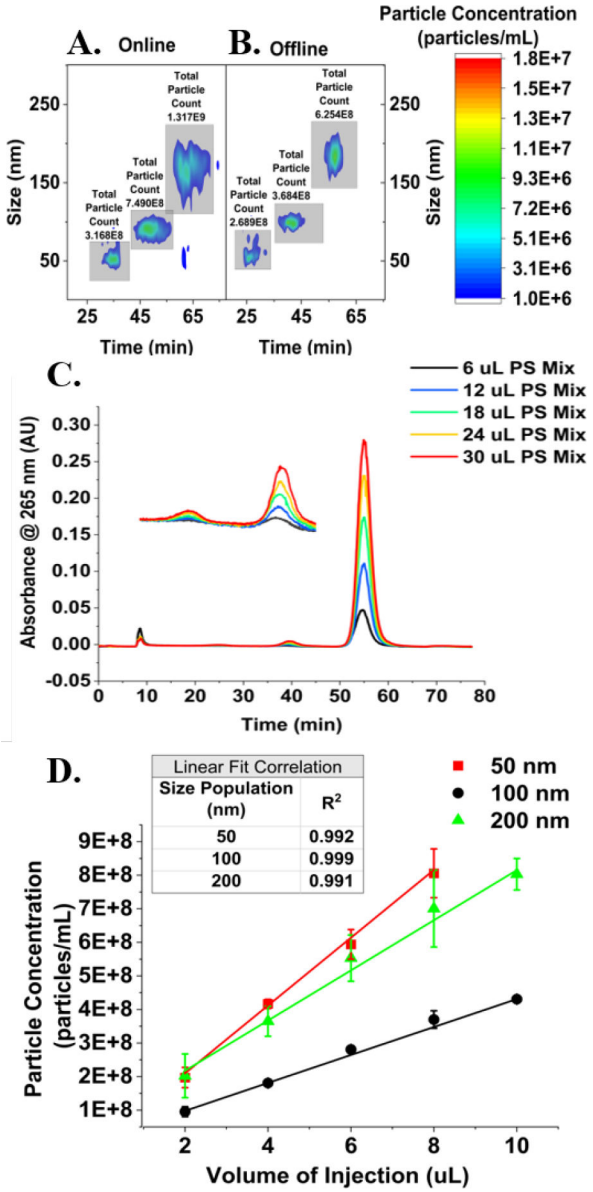

Figure 2.

Standard bead quantification tests. (A) Online NTA analysis and (B) offline NTA analysis of a 30 μL injection of a polystyrene bead mixture. (C) UV-Vis Absorbance (inset was the enlarged view for the peaks for 50- and 100-nm beads) and (D) NTA online quantification standard curve of increasing injection volumes of the polystyrene bead mixture, with the x-axis showing the volume of each type of beads added when preparing the mixture.

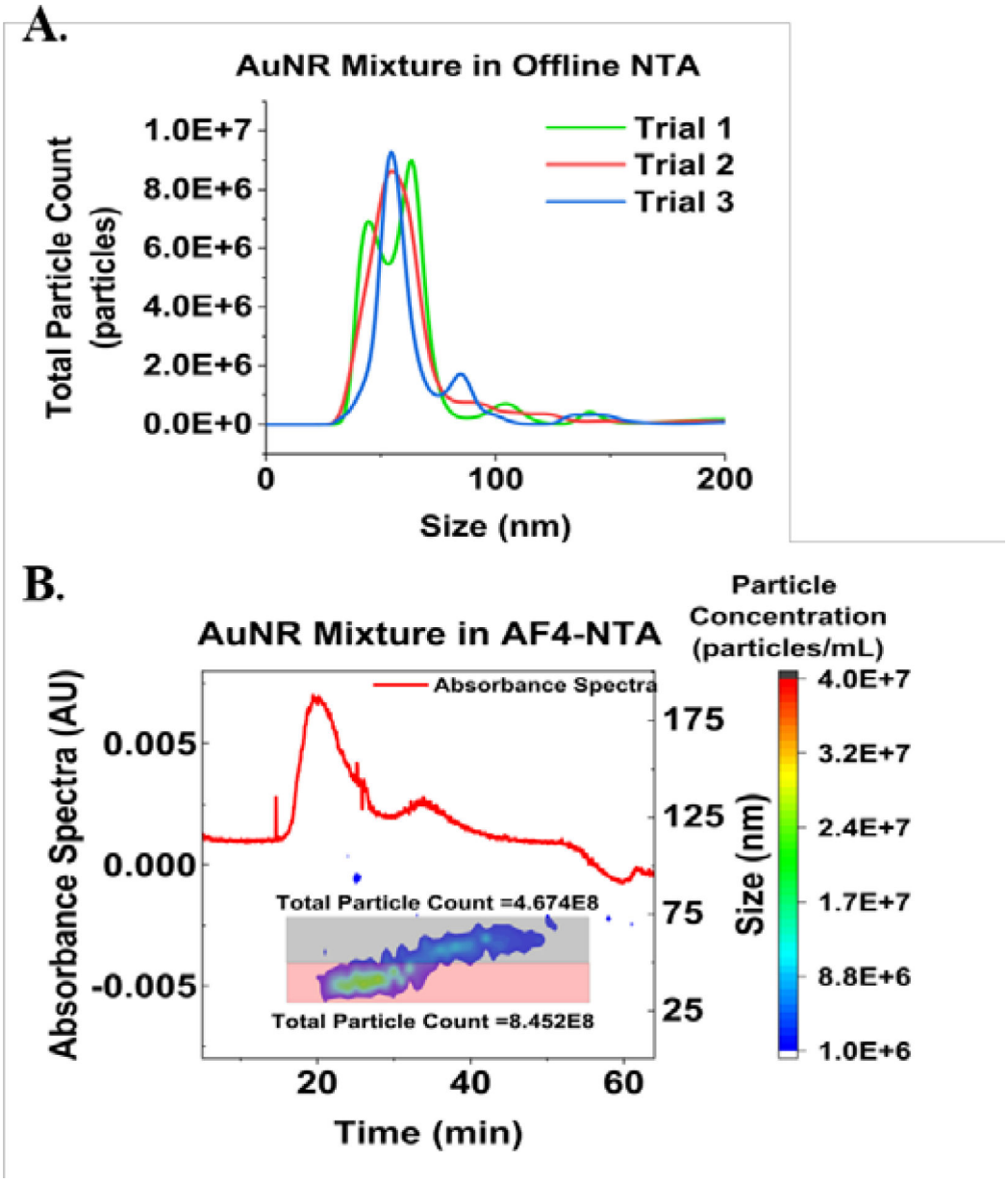

Figure 3.

Analysis of the mixture of the 103 × 18 nm and 46 × 17 nm AuNR diluted to 3.2×10^{8} and 2.36×10^{9} particles/mL, respectively, by (A) stand-alone NTA and (B) AF4-NTA.

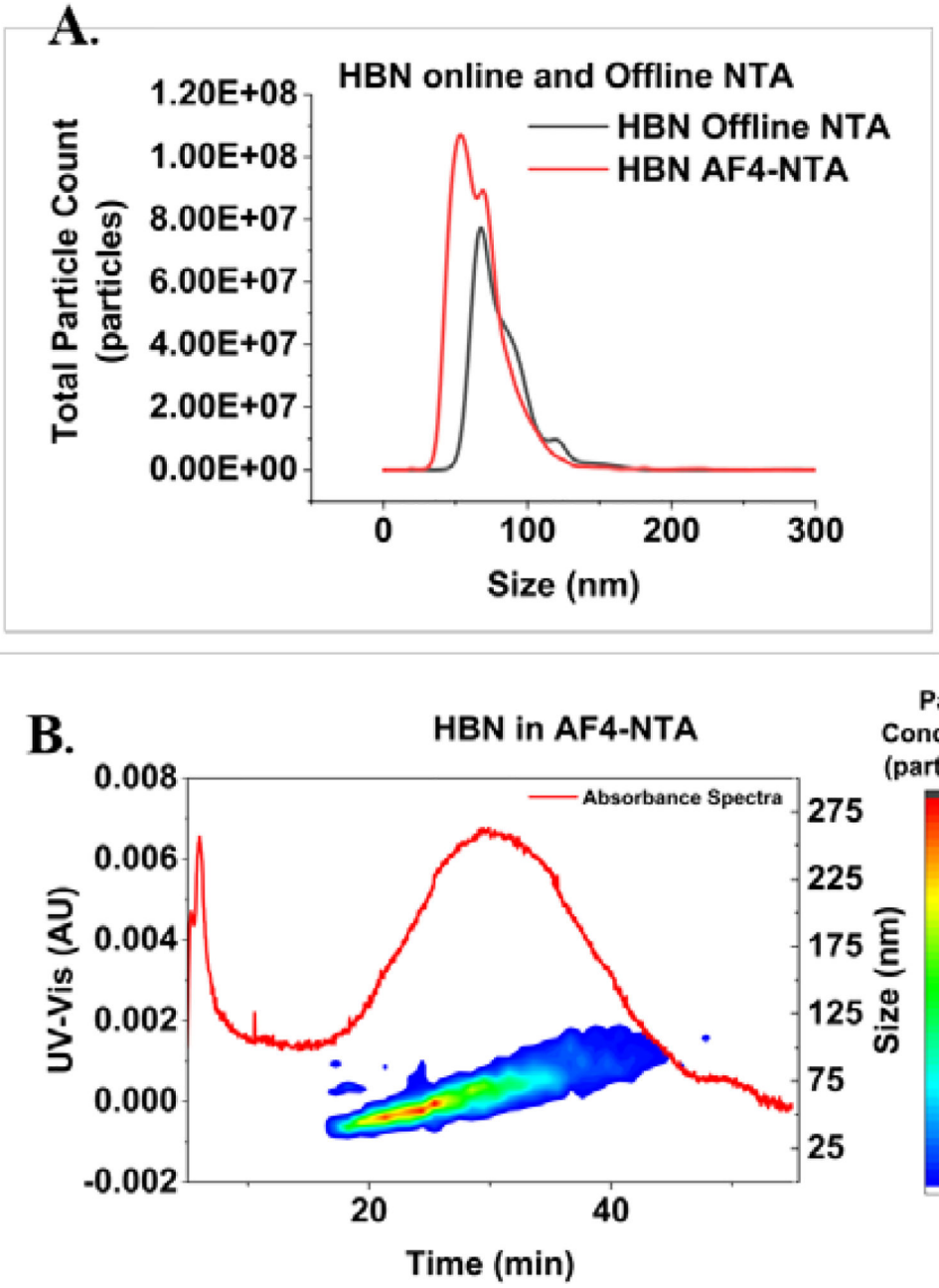

Figure 4.
Analysis of 500 ng/mL and 5 μg/mL hBN by (A) stand-alone NTA and (B) AF4-NTA.

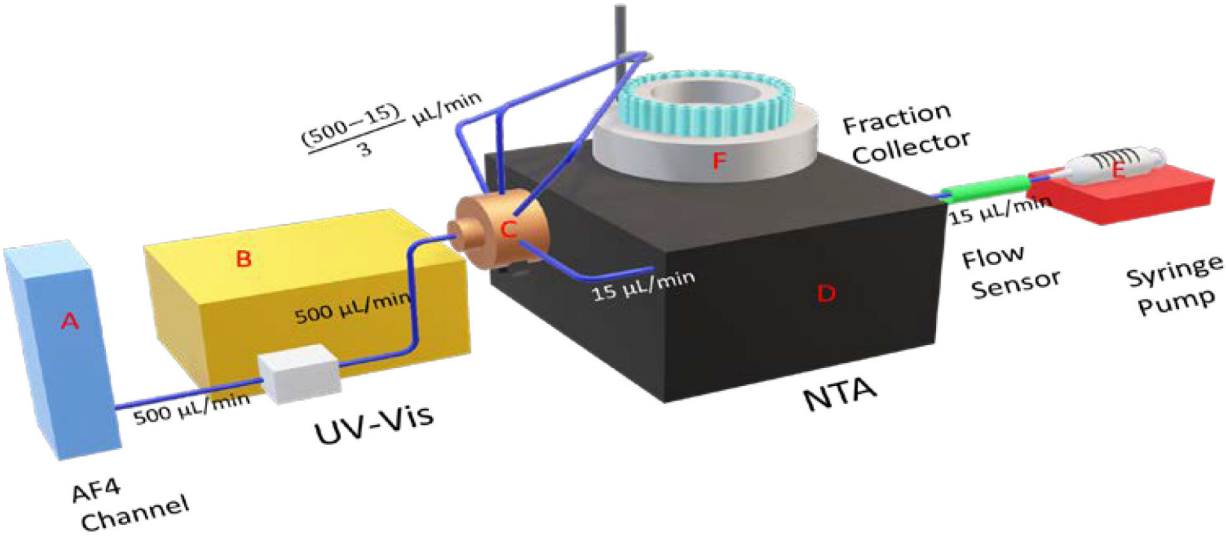

Scheme 1.

Schematic of AF4-NTA Connection. Eluent from the AF4 channel (A) is pushed at a constant 500 µL/min through the UV-Vis (B) until the flow is split at the splitter manifold (C). The line feeding the NTA is kept at a constant 15 µL/min by the flow sensor (D) and syringe pump (E). The remaining eluent lines feed the fraction collector. (F) The fraction collector flow rate can be calculated by:

$$FC\ Flow\ rate = \frac{AF4\ Detector\ Flow\ rate - NTA\ Detector\ Flow\ rate}{number\ of\ FC\ lines}$$

Table 1.

Total particle recovery comparison between injections of mixed populations of beads versus injections of single size populations. CV: Coefficient of Variability

SIZE (NM)	PARTICLE COUNTS BY SINGLE INJECTION	PARTICLE COUNTS BY MIXTURE INJECTION	CV (%)
50	5.055×10^8	5.526×10^8	4.72
100	4.364×10^8	4.132×10^8	0.601
200	1.277×10^9	1.169×10^9	4.68

Table 2.

Quantification and sizing results of offline NTA and AF4-NTA for analysis of AuNRs, as well as the Certificate of Authentication (COA) concentration and size information of the AuNRs provided by the manufacturer.

AuNR Size (nm)	Particle counts per 10 μL of Stock				Size Information			
	COA (particles)	Offline NTA (particles)	AF4-NTA (particles)	CV % Between Online and Offline	Hydrodynamic Diameter from COA (nm)	Offline NTA Hydrodynamic Diameter (nm)	AF4-NTA Size Mode (nm)	TEM Rod Length (nm)
47.6×18.0 nm	2.20E+09	1.77E+09	1.78E+09	0.28%	13	35	39.5	47.6
103.2×18.5 nm	3.20E+08	5.25E+08	5.91E+08	5.91%	19	53.5	57.5	103.2